High-resolution open-ocean temperature spectra

Hans van Haren, Louis Gostiaux

High-resolution open-ocean temperature spectra

Hans van Haren[1] and Louis Gostiaux[1,2]

Received 16 June 2008; revised 12 January 2009; accepted 16 February 2009; published 7 May 2009.

[1] Accurate (<1 mK) temperature sensors have been stiffly moored at ~1450 m in the open Canary Basin for 1.5 years while sampling at 1 Hz. The sensors were in an area where regular density steps occur. In this article, we investigate the variability of internal waves in such ''steppy'' environment. The waves vertically move layers of persistent temperature gradients for particular temperatures. The frequency (σ) spectra of temperature, and more clearly those of inferred vertical currents w, show an internal wave band IWB that extends from $0.97f < \sigma < N_t$, where f denotes the inertial frequency or vertical Coriolis parameter. Transition frequency N_t is higher than buoyancy frequency N, computed over large vertical scales $\Delta z = O(100)$ m. The extension of IWB beyond the traditional bounds [f,N] is probably due to small-vertical–scale layering ($\Delta z \approx 1$ m). The associated weak stratification between such thin layers provides small-scale $N_s \approx 4f_h$, where f_h denotes the horizontal Coriolis parameter. This minimum stable stratification N_s is associated with tilting of vorticity away from gravity, which causes the subinertial spectral extent to $0.97f$. Isothermal smoothing reveals details of coherent vertical internal wave and incoherent motions. The present w spectrum continuum of coherent IWB motions is not flat, as in previous near-surface observations, but linearly increases from $\sigma = f$ to a peak at $\sigma \sim 0.8$N. The coherence spectrum shows a weak, significant peak at approximately twice the local buoyancy frequency for $2.5 \leq \Delta z \leq 100$ m. Instead of dominant mode 1, zero phase difference, observed in IWB across the 130 m of observations, these super-buoyancy motions show mode 2 dominance, π phase difference.

Citation: van Haren, H., and L. Gostiaux (2009), High-resolution open-ocean temperature spectra, *J. Geophys. Res.*, *114*, C05005, doi:10.1029/2008JC004967.

1. Introduction

[2] Yearlong accurate measurements of open-ocean temperature variations that resolve internal waves and the largest turbulent overturning scales are rare. We use a unique data set from 54 temperature sensors covering 132.5 m in the vertical around 1450 m in the open Canary-Madeira Basin, North Atlantic Ocean, to study the characteristics of temperature and vertical isotherm displacements. The aim is to learn more about the precise spectral slope with frequency of temperature variance, quasi-potential energy and ''coherent'' vertical current spectra from moored sensors that are sampled at a rate of 1 Hz. Some comparison can thus be made with spectral studies like IWEX [*Briscoe*, 1975] that resolved more spatial but less temporal scales.

[3] The observations are from an area that is known for its steppy vertical density profiles [e.g., *Zenk*, 1970; *Howe and Tait*, 1970]. Typical step height of homogeneous layers is $O(10$ m), but varies considerably over time. In such layers, even negative gradients in both temperature T and salinity S can be found [*Howe and Tait*, 1970]. Here we consider particular internal wave propagation in relation to the steppy density distribution.

[4] Major contributions to the understanding of internal wave motions in the ocean interior and their spectra have been made in the 1970s. Kinematic modeling [*Garrett and Munk*, 1972, 1979] suggested vertical motion (w) spectra that are basically white in the internal wave band. Near-surface observations confirmed this model, with a small exception in a distinct peak near the buoyancy frequency [*Pinkel*, 1981]. *Pinkel* computed w spectra from the tracking of coherent isotherm displacements in his temperature observations, because the following of single isotherms proved not possible over any prolonged period of time. Likewise, *Cairns and Williams* [1976] demonstrated a nearly flat, significant coherence between isotherms up to 36 m apart in the frequency (σ) band $0 < \sigma < 0.5$N, where N denotes the buoyancy frequency computed over an unspecified vertical length scale. Vertical coherence was found peaking above the flat continuum just at 0.5N. *Cairns and Williams* [1976] used temperature sensors attached below a free-floating device. This setup smoothes the internal wave spectrum thus obtained as it mixes Eulerian and Langrangean measurements. Nevertheless, their results of linearly decreasing coherence with vertical separation compared reasonably well with other, Eulerian data. In addition, following a proposal by *Webster* [1972] and observations by *Siedler* [1974], vertical separation distance Δz, and thus coherence,

[1]Royal Netherlands Institute for Sea Research (NIOZ), Physical Oceanography, Texel, Netherlands.
[2]Now at Coriolis-Laboratoire des Ecoulements Geophysique et Industriels, CNRS, Grenoble, France.

0148-0227/09/2008JC004967$09.00

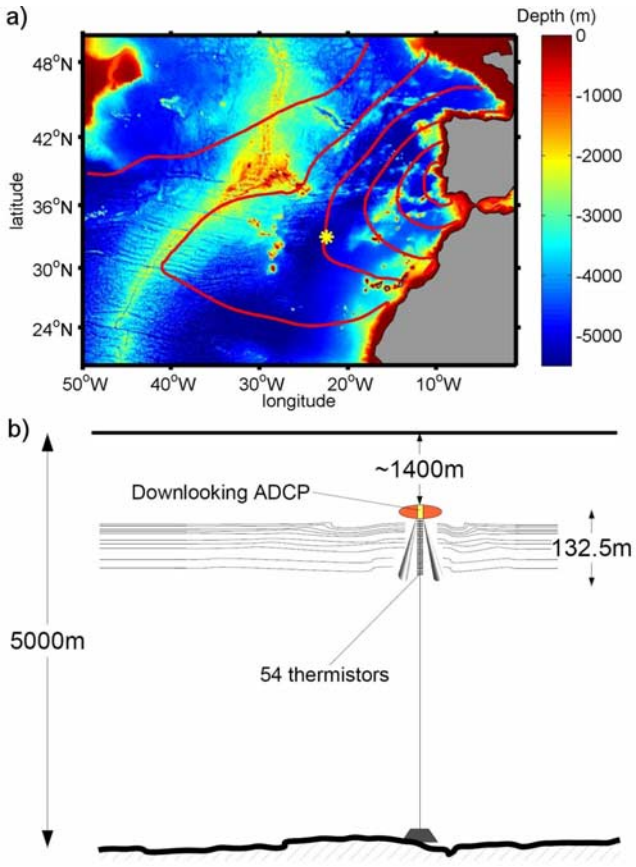

Figure 1. (a) Mooring site (asterisk), with annual mean salinity contours at 1400 m from World Ocean Atlas 2005 [*Antonov et al.*, 2006]. (b) Mooring diagram.

was assumed to vary like $\Delta z \sim \sigma^{-1}$ with frequency σ. However, *Wunsch and Webb* [1979] remarked that "many coherences are not monotonically decreasing functions of frequency", albeit without specifying to what extent.

[5] The present custom-made instrumentation is mounted on a specifically designed minimum drag mooring. This setup provides high-quality moored Eulerian spectra that are dominated by the internal wave band but which also resolve scales varying from long-term seasonal and mesoscale eddies to short-term energetic turbulence. Emphasis is on the effects of variations in background and local stratification in the form of multiple density layering on temperature, vertical current and coherence spectra. These data provide a refinement of our knowledge of ocean spectra, which started with the description by *Phillips* [1971] for step-like variations advected passed sensors fixed in space, "fine structure contamination", and by *Garrett and Munk* [1972] for internal waves. The time-depth series from which the present spectra are computed show an open ocean in a permanent state of predominantly internal wave motion, see a 113 s video representing real-time 50 days, out of 530, in the form of 8-hour frames of data at: http://nioz-hst.com/spip.php?article9#movie.

2. Data

[6] "NIOZ3" is a newly designed temperature sensor that is most commonly used in a string of multiple sensors. Being a follow-up of NIOZ1 and NIOZ2, it is also built to specifically study nonlinear internal waves and large-scale turbulent motions that may contribute to mixing and redistribution of material in the ocean. The NIOZ3 stand-alone sensors can sample temperature at a rate of 1 Hz for a period of 1.5 years and with accuracy better than 0.001°C. Their individual internal clocks are synchronized every 5 hours to a single standard via induction. The inductive principle is also used for communication with the sensors on board or in the laboratory.

[7] In order to learn more about open-ocean internal wave motions, 54 NIOZ3 sensors were taped to a steel mooring cable at 2.5 m intervals. This thermistor "string" was mounted directly below the elliptical top buoy of a 3800 m long mooring to the West of Madeira in the Canary Basin between May 2006 and November 2007 (see Table 1 for details; Figure 1). The heavy top buoy ensured wire tension exceeding 4000 N and the thermistor string can be considered as a stiff rod despite being mounted on a flexible steel cable. Typical horizontal currents are 0.15 m s^{-1}, but despite the long mooring line, pressure and tilt sensor information show <1.5° tilt angle and excursions across <1.2 m in the vertical and <100 m in horizontal directions. This is inferred from data sampled by the downward looking 75-kHz acoustic Doppler current profiler (ADCP) mounted in the top buoy, just above the NIOZ3 string. As a result, mooring motion due to current drag did not substantially affect the temperature observations.

[8] This first long NIOZ3 deployment was technically satisfactory. Some 18 sensors performed the entire 530 days of deployment and only 2 sensors failed. The remaining sensors nearly all performed well for the first year, but not very much longer due to battery problems that are now solved. Before and after the mooring period, NIOZ3 sensors were calibrated in situ by mounting them on a frame also holding a SeaBird 911 CTD. The two 1.5 years separated CTD profiles are also used to establish *T-S* relationships, which however cover a limited span of time, naturally.

3. Stratification: Background and Small-Scale Variations

3.1. CTD Data

[9] From hydrographic CTD observations in the Canary Basin it is known that NIOZ3 can reach through the lower part of relatively warm and salty Mediterranean outflow water, which commonly propagates in large subsurface eddies, "Meddies". Indeed, relatively large temperature

Table 1. Some Specifications of the NIOZ3 and First Yearlong Mooring Details

Accuracy	<1.0 mK
Sensor response time (τ)	0.25 s
Sampling frequency	1 Hz
Synchronization period	18,000 s
Number of sensors	54
Distance between sensors	2.5 m
Lowest sensor	1522 m
Water depth	5274 m
Latitude	33° 00.010′ N
Longitude	22° 04.841′ W
Deployment	10 June 2006
Recovery	22 November 2007

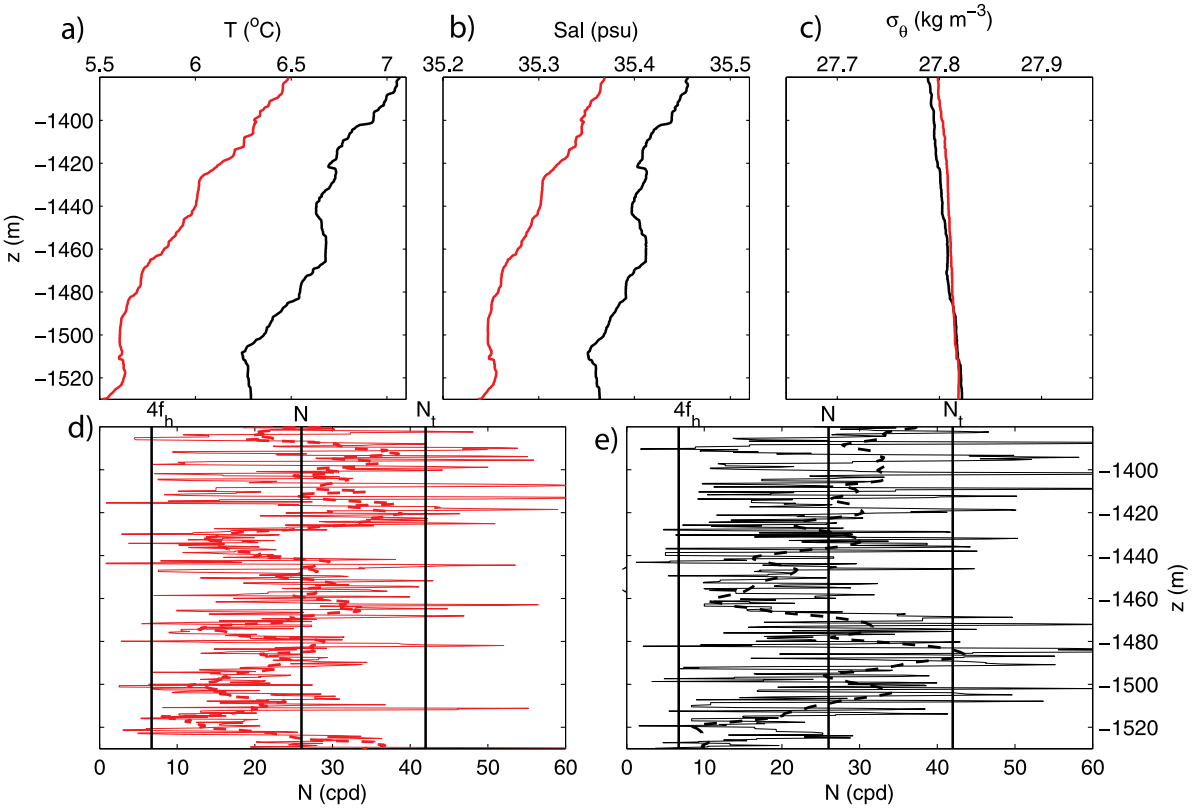

Figure 2. Detail of CTD profiles around the depths of NIOZ3 obtained just prior to mooring deployment (red) and after recovery (black). (a) Temperature. (b) Salinity. (c) Sigma-theta density anomaly referenced to the surface. (d, e) Small-scale buoyancy frequency using $\Delta z = 1$ m (thin solid) and larger scale using $\Delta z = 10$ m (dashed). In Figures 2a to 2c, the horizontal axis is constructed so that the scale represents approximately the same density change.

variations are found in the present NIOZ3 data, by up to 3.6°C. It is also clear in the record when a Meddy passes. Below such a meddy, but not necessarily uniquely related with Meddies, CTD data show numerous steps of alternating strong and weak vertical density stratification [*Zenk*, 1970; *Howe and Tait*, 1970; present Figure 2]. In Figure 2's depth range the large-scale density ratio of temperature over salinity contributions equals 2 and the Turner angle amounts about 75°. This associates the steppiness with moderate double-diffusive process or salt fingering, except for small unstable layers like near 1450 and 1520 m when the Turner angle is −110° for the same density ratio of 2.

[10] If these layers are "persistent" in space and time, say larger than several km horizontally and present over more than one inertial period, as suggested from observations by *Howe and Tait* [1970] and *Elliott et al.* [1974], they can support free internal waves up to the local buoyancy period $T_N = 2\pi/N$. Here $N = (-\mathrm{gdln}\rho/\mathrm{dz})^{1/2}$ denotes the buoyancy frequency, g the acceleration of gravity and ρ the density. It is hypothesized that the variation of high-frequency internal wave energy depends on the frequency distribution of $N(z)$: the $\mathrm{pdf}(N)(\sigma)|_{z1}^{z2}$ determined over depths $z_1 < z < z_2$. This will be investigated in section 4.

[11] The precise $N(z)$ depends on its vertical-length−scale Δz in association with a duration of time that should be larger than the particular internal wave of interest. Here we use high-resolution CTD data obtained at the end of the record that do not include, e.g., particular passages of Meddies: (1) an $N_s(z)$ distribution using arbitrary short-scale $\Delta z_s = 1$ m, which is the shortest scale over which N is realistically computable using CTD data stacked in 0.33 m vertical depth bins, (2) an $N_m(z)$ distribution using moderate-scale $\Delta z_m = 10$ m, (3) we compute a large-scale value $N_l(z)$ approximately across the range of NIOZ3 using $\Delta z_l = 100$ m. Henceforth, we imply with N without subscript $N \equiv N_l = \overline{N}_s = \overline{N}_m = 26$ cpd. The overbar denotes the averaging over the larger scale, which, implicitly is assumed to describe averaging over the longer time scales as well.

[12] As will be elaborated in section 4, the short-scale N_s distribution, with exclusion of statically unstable values, basically ranges between frequencies $4f_h < \sigma < N_t$, where N_t, equalling about half $N_{s,max}$, denotes a transition buoyancy frequency to, presumably, the buoyancy subrange of turbulence, and $f_h = 2\Omega\cos\varphi$ denotes the horizontal component of the earth rotation $\mathbf{\Omega}$ at latitude φ. The lower frequency bound requires measurement across $\Delta z = 1$ m of very weak density variations of $\Delta\rho = 2{-}3 \times 10^{-5}$ kg m^{-3}, which is approximately equivalent to $\Delta T = 1{-}1.5 \times 10^{-4}$°C. This is resolved by Seabird CTD sensors and commonly within its relative accuracy, provided raw data are used with only the necessary limited treatment and no filtering.

[13] With hindsight we define, $N_t \approx N_{m,max} \approx \overline{N}_s + 1\mathrm{std}(N_s) \approx \overline{N}_m + 2\mathrm{std}(N_m) \approx 0.55N_{s,max}$, as far as the relationship between N_s- and N_m distributions can be

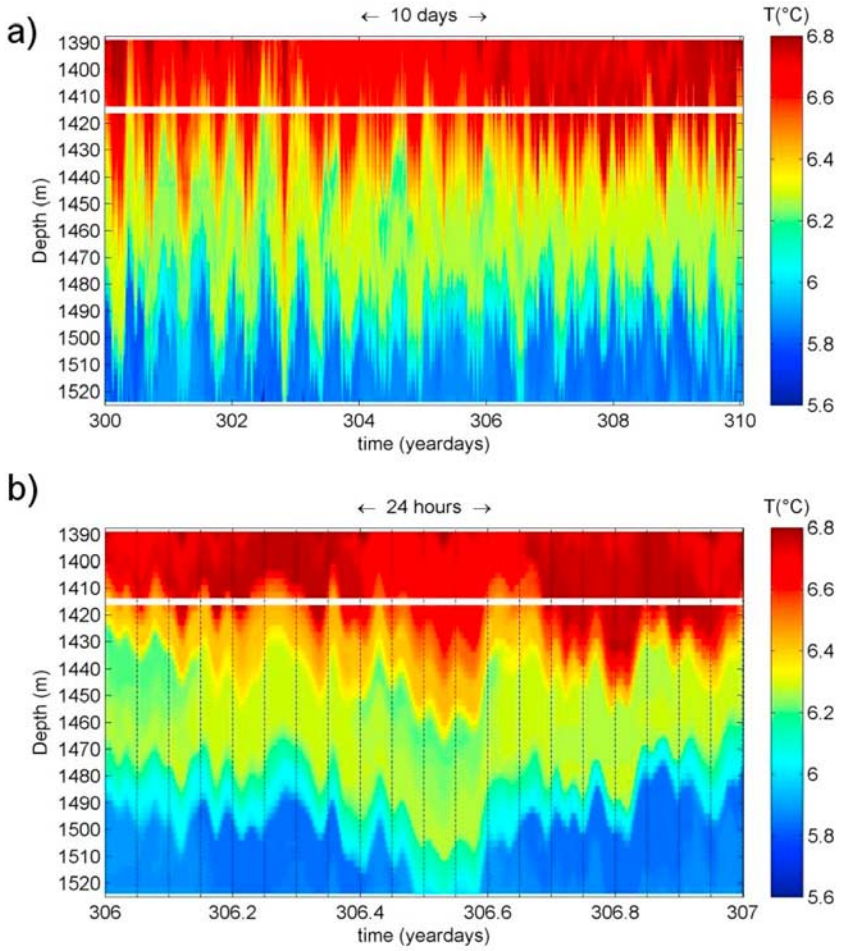

Figure 3. (a) Arbitrary 10 days of depth-time series of NIOZ3 temperature. (b) Arbitrary 1-day detail of Figure 3a. The vertical lines help verifying vertical phase variations.

established from the limited CTD data over the range of NIOZ3 (Figures 2d and 2e). A similar spread in N_s values was found at $\varphi = 30°$N above the foot of Great Meteor Seamount, also in the Canary Basin [*van Haren*, 2008a]. There, the pdf distribution of N_s values corresponded with the frequency distribution or spectrum of noise exceeding directly measured vertical current (w) data. However, the previously and presently observed range of stable N_s values barely reaches to the vertical Coriolis parameter, the inertial frequency $f = 2\Omega\sin\varphi$, which is the lower internal wave bound under large stratified conditions (Figures 2d and 2e; *van Haren* [2008a]).

[14] This is understood, because in weak stratification the horizontal Coriolis parameter becomes more and more important resulting in limiting frequencies like f_h, $2f_h$, $4f_h$ for "slant-wise convection" [*Straneo et al.*, 2002] in the direction of the earth's rotational vector, which is tilted away from gravity, except at the poles. These limiting frequencies are suggested to be due to different transitions from weak, just stable stratification in the direction of $\mathbf{\Omega}$ to homogeneous turbulence [*van Haren*, 2008b]. They depend on linear and nonlinear mixing regimes, following a formulation in critical gradient Richardson numbers. In turn, the limiting frequencies determine the internal wave spectral continuum, as will be demonstrated in section 4, especially for $\sigma = 4f_h$.

3.2. NIOZ3 Temperature Variations

[15] The steppy layering in vertical density and $T(z)$ profiles of CTD data is also visible in NIOZ3 temperature observations. Examining an arbitrary 10-day portion, one clearly observes variations in temperature transitions (Figure 3a). Even clear inversions are observed, with negative vertical temperature gradients $dT/dz < \Gamma \approx -1.7 \times 10^{-4}$ °C m^{-1}, thus exceeding the adiabatic lapse rate in amplitude, e.g., on day 304 around 1450 m. These negative temperature gradients must be compensated by salinity, although we lack observational evidence.

[16] The layers of varying temperature transitions move up and down in an apparent regular fashion, both with tidal periodicity (Figure 3a) and with near-buoyancy periodicity (Figure 3b). Vertical amplitudes amount up to several 10s of m. To first order, motions are in phase over the range of observations, but deviations also occur commonly, e.g., on days 306.25 and 306.65 (Figure 3b). The large moving up and down questions the precise nature of the layers and their persistence with time: as the diffusive process can be ambiguous in small layers (Figure 2), it is remarkable how it can survive these internal wave motions.

[17] Each of the tidal and buoyancy periods shows slight differences in the layers in terms of precise thickness and temperature gradients. Plotting time series of the latter as a

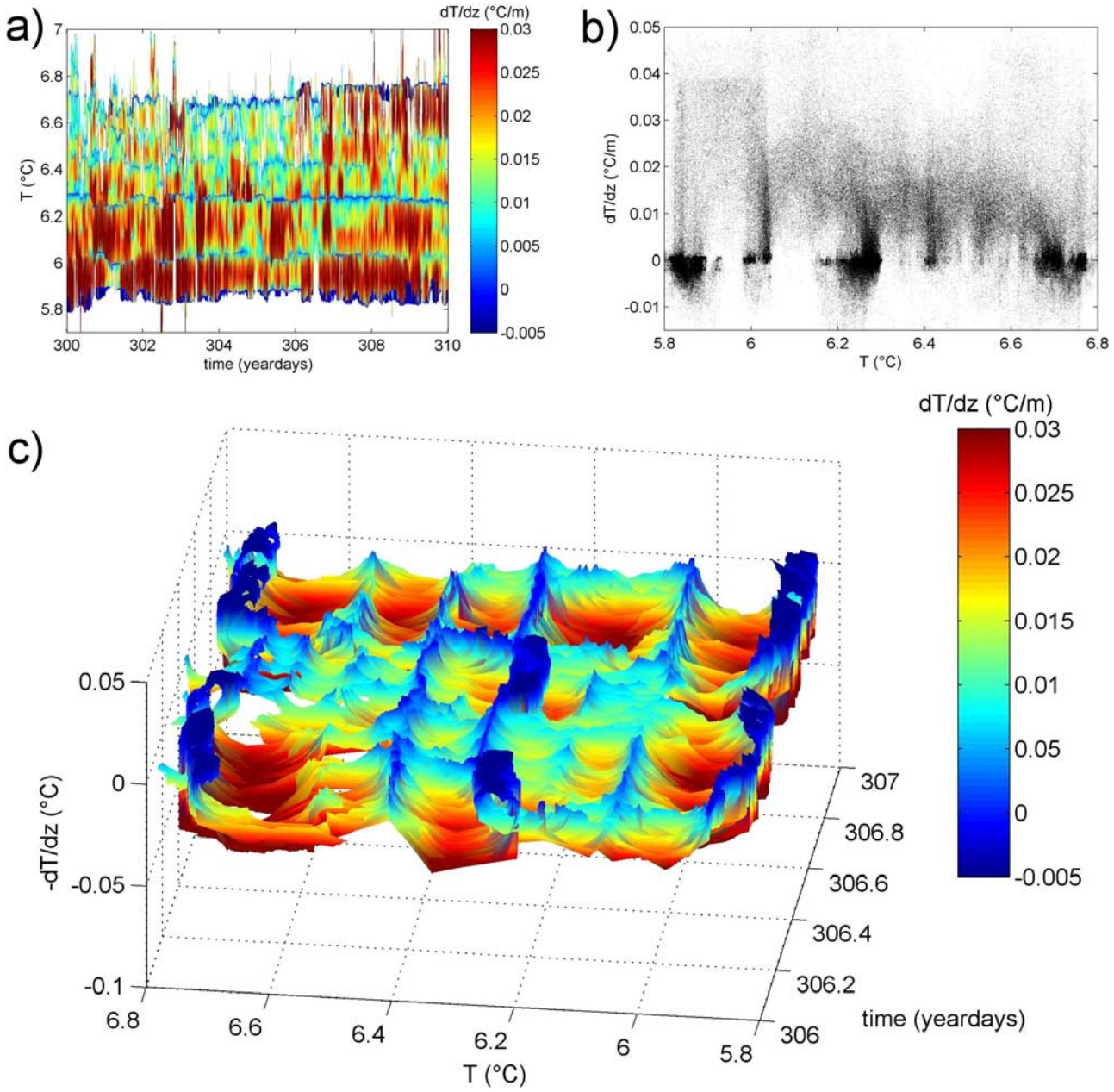

Figure 4. Time series of vertical temperature gradients as a function of temperature in different formats for the same periods as in Figure 3. (a) Full 10-day period contouring of dT/dz. (b) Scatterplot of dT/dz versus T for the same 10-day period. (c) Three-dimensional view of dT/dz contours for 1-day period as in Figure 3b.

function of T, one observes "persistently" high, or low, dT/dz for particular T values (Figure 4). With small deviations the persistency lasts at least a day, mostly several days, and far beyond the buoyancy timescale. This suggests true layering and confirms previous observations [*Elliott et al.*, 1974]. The layering in the examples of Figure 4 shows especially tight T values for dT/dz = 0 (Figures 4a and 4c). This shows in Figure 4b as well-localized points with arcs of non-zero temperature gradient values in between. Of course, these arcs spread over more than one value, but in time their peak values seem to organize in tidal periods and in periods of about 0.1 day duration showing as valleys in Figure 4c. This periodicity is about half the typical bouyancy period of waves (Figure 3b). Assuming a tight T-S relationship, as observed in the limited CTD data (Figure 2), lasting "persistent" periods of several days, we use NIOZ3 T data as tracers for the density structure. Thus we investigate below internal waves that are supported by this layered vertical density structure.

4. Spectral Observations

4.1. Overview

[18] The interior Madeira-Canary Basin 1.5-year mean temperature spectra are dominated by a weakly sloping plateau that roughly ranges from inertial frequencies to just

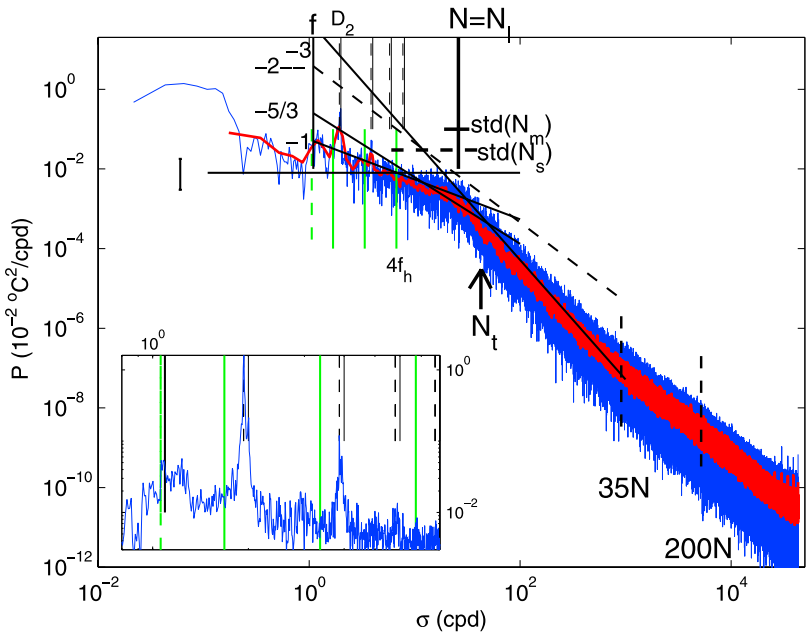

Figure 5. Moderately (blue) and heavily smoothed (red) 1-Hz temperature data from a single NIOZ3 sensor at 1405 m. A subset between arbitrarily chosen days 280 and 380 is used for computational purposes. The 95%-significance level is shown by the small vertical bar for the heavily smoothed spectrum. The black straight slopes indicate σ^{-3} fall-off rate with frequency, $\sigma^{-5/3}$, σ^{-1} and flat σ^{0}. The canonical slope σ^{-2} is dashed. The vertical green lines indicate frequencies f_h, $2f_h$ and $4f_h$, the black dashed ones $M_{2,4,6,8}$ and solid ones $S_{2,4,6,8}$. A suggested transition frequency N_t is indicated by an arrow. Other transition frequencies, 35N and 200N, are discussed in the text. Large-scale $N = N_l$ and the moderate-scale extend ±1 std(N_m) are indicated by a solid cross, with the dashed horizontal line indicating ±1 std(N_s). D_2 indicates semidiurnal frequency band rather than particular harmonic frequencies within this band. Insert shows low-frequency part of the IW band in detail using full-length time series of 530 days subsampled for computational purposes at 0.2 Hz. The green dashed line is at $0.97f$.

below the large-scale buoyancy frequency (Figure 5). This plateau stands out like an inclined top hat for $f \sim< \sigma \sim< N$ above an otherwise monotonically decreasing spectrum.

[19] A few peaks extend above this "internal wave IW band" plateau, the largest being the semidiurnal peak in the moderately smoothed spectrum, further a fourth-diurnal peak and small peaks are found near f and the ter-diurnal band. The semidiurnal peak is about a decade below the level of very low frequency, e.g., seasonal and Meddy, variations at $\sigma = 0.01-0.03$ cpd. None of these peaks resembles a line spectral peak that represents a purely deterministic signal. All represent finite width bands or partially "stochastic" signals. In the time domain this shows as the familiar "intermittent" appearance and disappearance of particular waves and wave groups, even for the semidiurnal tidal variations [*van Haren*, 2004]. For this intermittency, typically 7–10 waves occur in a group, but modulation amplitudes vary, apparently randomly (Figure 3). In Figure 5, the smallest spectral "peaks" are indistinguishable from the surrounding spectral continuum, when regarded as purely statistical rather than quasi-deterministic variations.

[20] The continuum internal wave band power spectral slope $\partial P/\partial\sigma$ amounts about −1, so that

$$P \propto \sigma^{-1}, \qquad \text{for } f < \sigma < \sim 0.25 - 0.35N,$$

except for a few gaps of which the largest is found just above f. This slope is also assumed to be the typical spectral slope of another class of intermittent signals providing broadband "noise" at low frequencies [*Schuster*, 1984]. This intermittency describes the occurrence of a signal which alternates between long regular phases and short irregular bursts. In practice, its frequency domain is limited over 2–3 decades [*Schuster*, 1984].

[21] At the high-frequency end of the internal wave band, the transition to a steeper slope is not well defined in the T spectrum and certainly not statistically significant. In a less smooth spectrum the σ^{-1} slope seems to extend to ~0.7N. However, by using straight slopes in the log-log plot a weak, nonsignificant deviation from the σ^{-1} slope to the near N "bulge" occurs around $\sigma = 4f_h \approx 0.25$N.

[22] As mentioned above, this "internal wave continuum slope" includes, besides a weaker ter-diurnal peak, the near-inertial peak, which is thus not negligible, despite the traditional idea that near-inertial internal wave motions are purely horizontal and thus not reflected in vertical T variations. If produced via advection by horizontal inertial currents having amplitudes of ADCP-observed 0.01–0.02 m s^{-1}, the NIOZ3-observed $T(f)$ would require horizontal gradients of $dT/dx,y \approx 10^{-4}$ °C m^{-1}. Although we lack spatial information, this value seems too large for large-scale ocean frontal phenomena and only occasionally some small-scale,

possibly internal wave-induced, variations have been observed of the same size [*Elliott et al.*, 1974].

[23] After closer inspection, the T spectra extend to subinertial frequencies just down to $\sigma = 0.97f$ (Figure 5 insert: dashed green line), which is equal to the nontraditional lower bound [*LeBlond and Mysak*, 1978; *Gerkema and Shrira*, 2005] $\sigma_{\mathrm{lo}}(N) = [s-(s^2-f^2N^2)^{1/2}]^{1/2} < f$ of the inertio-gravity wave band for $N = 4f_{\mathrm{h}}$. Here $\mathrm{s} = [\mathrm{N}^2 + \mathrm{f}^2 + \mathrm{f}_{\mathrm{h}}^2]/2$, for north-south propagating waves. This observed subinertial peak is significantly distinguished from the nearest diurnal tidal harmonic constituent K_1. It confirms a relationship between internal waves and step formation in the ocean as suggested from a stability/shear analysis [*van Haren*, 2008b]. The slight deviation away from f to subinertial frequencies is due to the horizontal component of the earth rotation, or the effect of a tilting of vorticity away from gravity and in the direction of the Earth rotational vector.

[24] On the other side of the internal wave band, the roll-off near N is rather clear cut and drops in a steep descent precisely at large-scale N. The roll-off ends abruptly at transition frequency N_t. The super-buoyancy range slopes initially like,

$$\mathrm{P} \propto \sigma^{-2.5}, \qquad \text{for } \mathrm{N_t} < \sigma < \sim 35\mathrm{N},$$

before changing to a less steep,

$$\mathrm{P} \propto \sigma^{-5/3}, \qquad \text{for portions in the range } \sim 35\mathrm{N} < \sigma < 200\mathrm{N}.$$

This approximates the canonical turbulence slope, provided we assume Taylor hypothesis to be valid for ''constant'' large-scale advective motions and the frequency domain is linearly transferred to a horizontal wave number ''k'' domain. In the k domain, a temperature variance spectral slope of $\sim \mathrm{k}^{-3}$ is considered to represent the buoyancy subrange, as conjectured theoretically [*Weinstock*, 1985] following microstructure observations [*Gregg*, 1977] although an alternative of $\sim \mathrm{k}^{-7/3}$ has been proposed theoretically [*Holloway*, 1986]. In the same domain, $\mathrm{k}^{-5/3}$ slope formally holds for inertial subrange temperature, or any other scalar variable [*Tennekes and Lumley*, 1972].

[25] Implied turbulent dissipation rates ε are hard to determine using the present data set. Bluntly computing temperature gradients between two sensors gives typical values for temperature ''dissipation'' $\chi_T = O(10^{-11}\ ^\circ\mathrm{C}^2\ \mathrm{s}^{-1})$, using parameterization by *Oakey* [1982]. These values are very low and presumably due to the relatively high vertical-scale limit of 2.5 m, which causes the Batchelor spectrum to be poorly resolved. Alternatively, one could try to estimate ε from the $T(\mathrm{k})$ spectrum, using Taylor hypothesis, but then one requires to find the appropriate Ozmidov length-scale λ_{O} to find the inertial convective subrange ICS cutoff. The sensitivity to such cutoff, in combination with the fuzziness of the spectral slope transitions, does not allow precise estimates and requires more attention, beyond the scope here. As a first attempt, taking the ICS cutoff near $\sigma = 35$ N, transforming $T(t)$ to $T(\mathrm{x,y})$ using low-pass filtered currents, one finds, following parameterization by *Sreenivasan* [1996], an estimate of $\varepsilon = [\mathrm{E_c}/\mathrm{C}_\theta\Gamma_{\mathrm{m}}(N_{\mathrm{l}}/\mathrm{g}\alpha)^2]^{3/2} \approx 1.2 \times 10^{-9}$ W kg^{-1}. Here we used spectral variance $\mathrm{E_c} = 1.5 \times 10^{-7}\ ^\circ\mathrm{C}^2\ \mathrm{m}^{-1}$ at the ICS cutoff frequency, Obukhov-Corrsin constant $\mathrm{C}_\theta = 0.4$ and mixing efficiency $\Gamma_{\mathrm{m}} = 0.2$, and the large-scale buoyancy frequency value scaled with thermal expansion coefficient α and g. Using the above values, the vertical eddy diffusivity is estimated, following *Osborn* [1980], $\mathrm{K} = \gamma\varepsilon/\mathrm{N}^2 \approx 4.5 \times 10^{-5}\ \mathrm{m}^2\ \mathrm{s}^{-1}$. This value is higher by a factor of 2–4 than free-falling probe estimates of open-ocean diffusivity, but rather typical for internal wave induced mixing and to within a factor of 3 confirmed with limited CTD/LADCP observations (not shown). Likewise, a reasonable estimate is obtained for $\lambda_{\mathrm{O}} = (\varepsilon/\mathrm{N}^3)^{1/2} \approx 3$ m. However, we caution the use of the above estimates, as the robustness of spectral cutoff and underlying models are uncertain. Values are probably not better than to within a factor of 10.

[26] In the present data, the classic -2 slope [*Garrett and Munk*, 1972] is not commonly observed, except in the small frequency transition between the above last two slopes, and for very high frequencies:

$$\mathrm{P} \propto \sigma^{-2}, \qquad \text{for } 200\mathrm{N} < \sigma < \mathrm{Nyq},$$

where Nyq denotes the Nyquist frequency. The white noise 0 slope commences only very close to Nyq, which demonstrates an extremely low variance, complying easily with noise level <0.001°C, and amounting about 0.5 mK on average. This average value is still mainly due to natural variance and calm episodes with 50 μK instrumental noise levels have been observed in the record. This demonstrates the high performance of NIOZ3.

4.2. Coherent and Incoherent Temperature Scales

[27] We commence investigation of vertical coherence of internal motions by comparing NIOZ3 records from different levels. At $\Delta z = 2.5$ m vertical distance we compute $\Delta T = T(z)-T(z-\Delta z)$, which we consider as tracer here but which can be used as a reasonable estimate for small-scale $\mathrm{N_s^2}$ variations. It is the best estimate NIOZ3 data provide for density steps of less than 2.5 m and their variations with time. This ΔT spectrum is markedly different from the T spectrum (Figure 6). The variance of ΔT, $\mathrm{var}(\Delta T) \ll \mathrm{var}(T)$ for $\sigma \leq N_t$ and $\mathrm{var}(\Delta T) > \mathrm{var}(T)$ for $\sigma > N_{\mathrm{s,max}}$, the maximum value found for small-scale buoyancy frequency in the range of Figures 2d and 2e. The transition is rather sharp across frequencies $N_t < \sigma < N_{\mathrm{s,max}}$, at which T spectral $\partial\mathrm{P}/\partial\sigma < -3$. At $N_{\mathrm{s,max}}$, the T spectrum transits to the aforementioned $\sigma^{-2.5}$ slope, while beyond that frequency the ΔT spectrum gradually adopts a σ^{-3} slope.

[28] For most $\sigma > N_{\mathrm{s,max}}$, $\mathrm{var}(\Delta T) = (2 \pm 0.5)\mathrm{var}(T)$, which suggests that motions at these frequencies are completely uncorrelated. After all, the value of 2 is exactly the variance increase factor for two purely random stochastic signals subtracted from each other. The steep slopes of about σ^{-3} and transition to $\sigma^{-5/3}$ fall-off rate for ΔT remain the same as for the T spectrum, with the exception of the roll-off phase of the ΔT spectrum between about 100 and 200 cpd (cycles per day).

[29] On the other side, for $\sigma \leq 0.4 \pm 0.1N_t$ $\mathrm{var}(\Delta T) < 0.1\mathrm{var}(T)$ and for $\sigma \leq 4f_{\mathrm{h}}$ $\mathrm{var}(\Delta T) = 0.02\mathrm{var}(T)$ on average, from which it is concluded that variations at these frequencies are coherent across $\Delta z = 2.5$ m. Thus, within the band of, single CTD determined, $N_{\mathrm{s}} \pm 1\mathrm{std}(N_{\mathrm{s}})$ distribution a

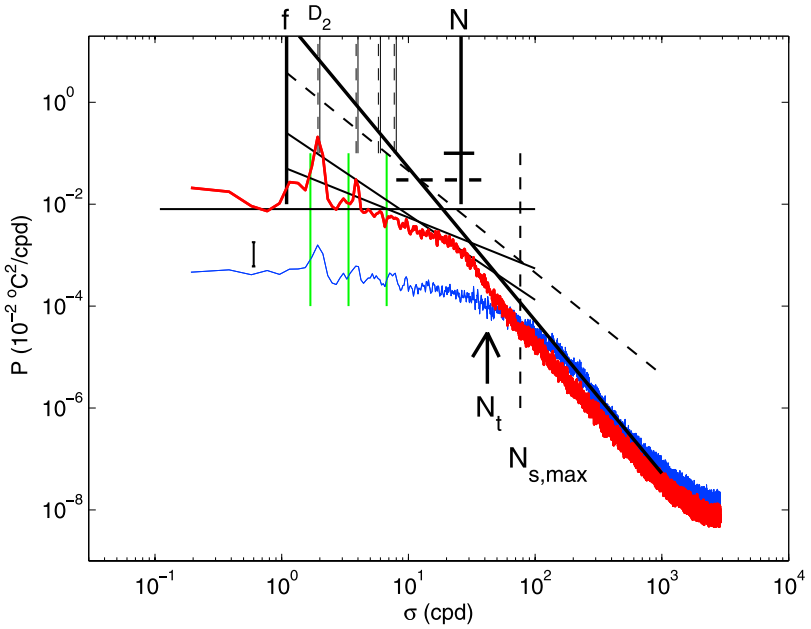

Figure 6. Spectra of first 180 days, before the passage of an intense Meddy, of temperature data subsampled at once per 15 s and observed at 1390 m (red) and of temperature difference between 1390 and 1392.5 m (neighboring sensors, blue).

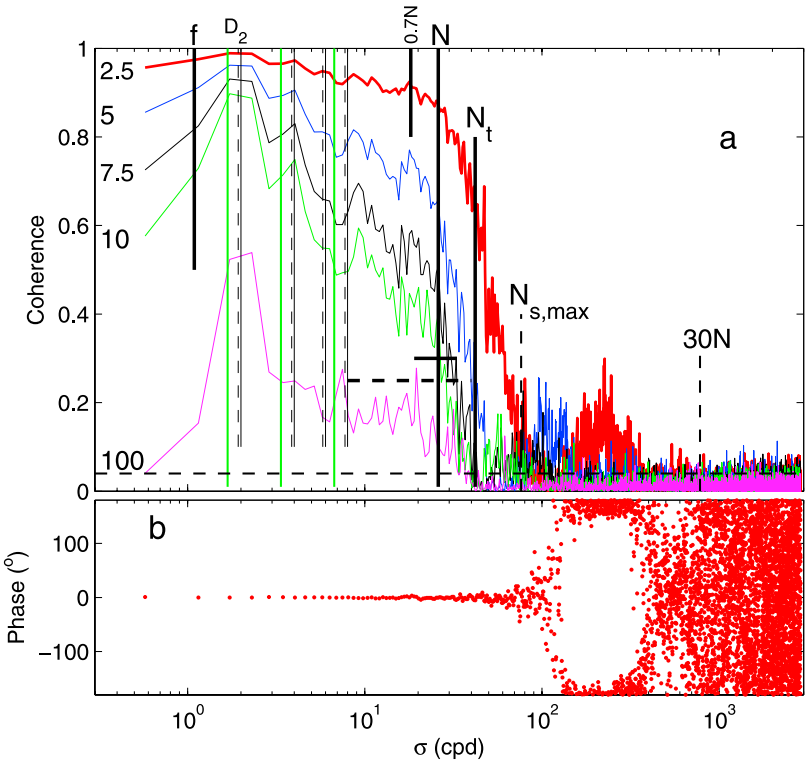

Figure 7. (a) Coherence spectra of first 180 days of temperature data subsampled at once per 15 s and observed between 1390 m and sensors at 1392.5 m (red), 1395 m (blue), 1397.5 m (black), 1400 m (green), and 1490 m (purple). The vertical distances between the sensors are indicated to the left in meters, the horizontal dashed line indicates the approximate 95% confidence level. (b) Associated phase, but for red spectrum only, between sensors at 1390 and 1392.5 m. Note the flip crossing from −180 to +180°.

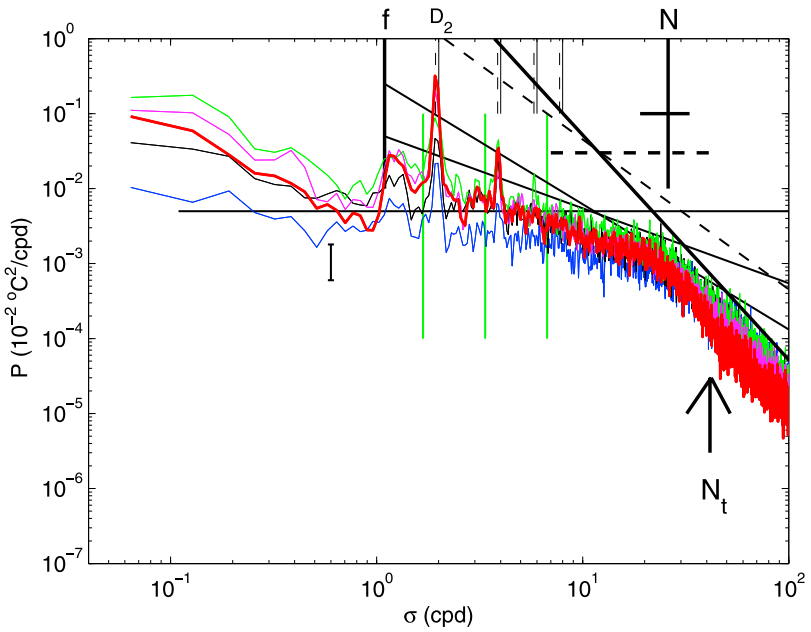

Figure 8. Temperature difference spectra for first 180 days records and subsampled at once per 15 s, with the same red T spectrum as in Figure 4 for reference. Temperature differences are computed between 1390 and 1400 m (blue), 1410 m (black), 1490 m (green), and 1517.5 m (purple).

rapid discrepancy between var(ΔT) and var(T) is observed, while for $\sigma < 4f_h$ this discrepancy barely increases for decreasing frequencies. The ΔT spectrum is nearly flat for $\sigma \leq N$, albeit not representing instrumental white noise, with no distinct transition between super-inertial and sub-inertial frequencies and with just three statistically nonsignificant "peaks" around D_2, the semidiurnal frequency band, fourth-diurnal band D_4 and $\sigma = 4f_h$. Within the continuum, values at $\sigma = f_h$, $2f_h$ and $4f_h$ are relatively large compared to those in the T spectrum, whereas those within "bands" of f, D_2 and D_4 are relatively small.

[30] These observations are largely confirmed by coherence spectra across several vertical distances (Figure 7). With increasing vertical distance between the sensors the internal wave band level of coherence decreases and the frequency range of significant coherent values narrows, both at the near-inertial side and, more clearly, at the near-buoyancy side. In all cases, the coherent internal wave band part is associated with a mean of 0° phase difference, for the half-year average. For $\Delta z = 2.5$ m vertical distance the coherence drops below the 95% significance level at "incoherence frequency" $\sigma_{incoh} = (1 \pm 0.2)N_{s,max}$, throughout the moored sensors array, while $\sigma_{incoh} \approx N_t$ for $\Delta z \geq 10$ m.

[31] In comparison with observations by *Cairns and Williams* [1976] the internal wave band coherence spectra are not flat in NIOZ3 data, presumably due to large tidal influence. For $\Delta z \geq 5$ m a little hump is observed around $\sigma = 0.7 \pm 0.05$ N, in both data sets. It is unclear why enhancement is found at this frequency; and whether it may be attributable to subharmonic resonance.

[32] Remarkable in the NIOZ3 data (Figure 7) is that beyond the buoyancy frequencies, significant coherence levels are also found in a narrow frequency band for all depth intervals. This is not an artifact, as the sensors are completely independent. The super-buoyancy coherence is found approximately between $2\sigma_{incoh} < \sigma < 3{-}4\sigma_{incoh}$. The associated phase is very close to a "mode 2 character" over the range of observations, 174 ± 12° for $2.5 \leq \Delta z \leq 5$ m, and similar mean values but larger errors for larger vertical distances. The nearly 180° phase difference explains why in this frequency range the vertical difference spectra are exceeding the individual temperature spectra by a factor of more than 2 (up to ~2.5; Figure 6), not just attributable to random signals, but partially also to coherent out-of-phase signals. These high-frequency super-buoyancy "waves" are likely due to kinematics by the vertical N-wave motion of thin, <2.5 m mainly, layers past the sensors. It may also be due to coupling to buoyancy frequency motions via wave-wave interactions, as observed in the laboratory previously [*Davis and Acrivos*, 1967], but it seems less dominant than kinematics here. Further in the coherence record, barely significant coherence is found at even higher frequencies, with distinguishable coherent 0 phase difference up to $\sigma \sim 20{-}25$ N, for $\Delta z = 2.5$ m only.

[33] Also in vertical temperature difference spectra it is observed that the internal wave and subinertial bands' vertical coherency is rapidly decreasing for increasing Δz (Figure 8). Already at $\Delta z = 20$ m the continuum var(ΔT) ≈ var(T) for $\sigma \leq N_t$, except in frequency bands like $\sigma \ll f$, $\sigma = D_2$ and D_4, but, surprisingly, also near $\sigma = f$ and not near N. Whereas large vertical coherent scales in temperature variations are expected for near-N variations [Cf., *Cairns and Williams*, 1976], and which are indeed observed in short portions of the present time series showing at best phase rather than amplitude shifts, e.g., day 306.45 in Figure 3b, it surprises that they do not show on a regular basis in the time mean. Large vertical coherence is less known for near-f variations that in the mean have vertical coherent scales exceed $\Delta z > 10$ m, to first order.

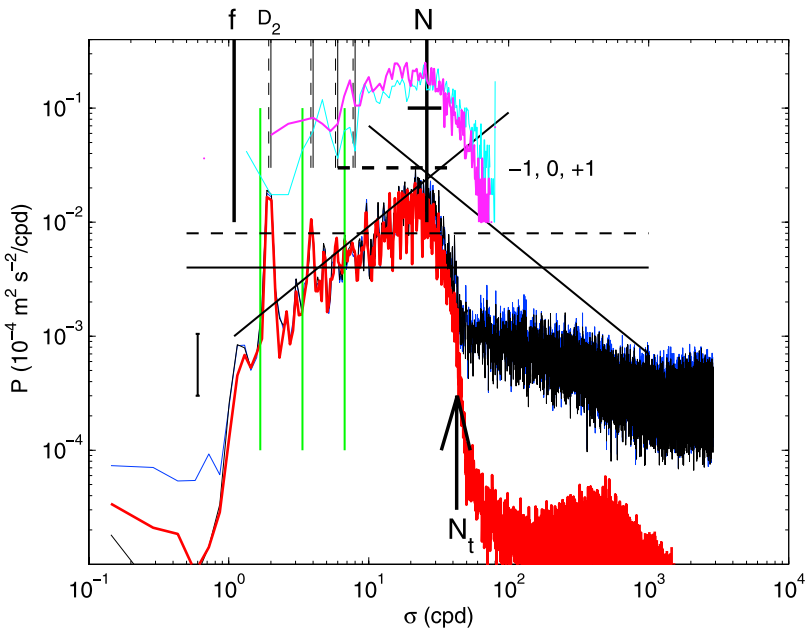

Figure 9. In red, spectra of vertical current computed from vertically coherent isotherm displacements using first 2 months of data subsampled at once per 15 s. In this period, little or no temperature inversions are observed. The isotherm displacement is determined over a 30-s interval, hence the high-frequency drop-off for $\sigma > 300$ cpd as if low-pass filtered. In blue, $w_T = -\partial T/\partial t/\langle \partial T/\partial z \rangle$ computed using time steps of 15 s and observed at 1390 m; in black, $w_T = -\partial T/\partial t/\partial T/\partial z(t)$. Arbitrarily off-set are very-small−scale buoyancy frequency distributions, which are computed from 0.33 m CTD data for the ranges 800 and 1500 m (light blue, data after recovery) and 1100 and 1800 m (purple, data before deployment). They, naturally, reach up to $N_{s,max}$.

[34] The near-f peak in T spectra already points at either advective temperature variations or temperature variations due to near-inertial convection in the direction of the earth's rotation axis across weakly stratified layers for "N" = $4f_h$ [*van Haren*, 2008b], the quotes denoting unknown vertical length scale. As such layers generally have much larger vertical extent than the well-stratified layers between them (Figures 2 and 3), this may explain the relatively large vertical coherent scale for near-f variations as inferred from the ΔT spectra (Figure 8).

[35] For increasing Δz up to about the NIOZ3 range it is observed that var(ΔT) $\approx$ 2var(T) or vertical incoherency is reached for $\Delta z \approx 50$ m, except at $\sigma \ll f$, and bands D_2 and D_4. In these exceptional frequency bands var(ΔT) $\approx$ 0.5var(T), so that their vertical scales exceed the NIOZ3 range employed here. However, this exceeding is not by an enormous amount and it is estimated that vertical incoherency is found for $\Delta z = 200-500$ m in these bands. It is noted that largest var(ΔT) is found for $\Delta z = 100$ m, not for the maximum range. This may be due to the vertical temperature stratification nonuniform decrease with depth.

[36] The above variations imply a nonmonotonic decrease of vertical separation with frequency, certainly not behaving like −1 in log-log slope, as already suggested by *Wunsch and Webb* [1979].

4.3. Large-Scale Isotherm Displacements and Vertical Currents

[37] In a different way, motions that are vertically coherent over the entire NIOZ3 range are determined for each time step by computing the vertical displacement over a time interval dt = 30 s that correlates best for all sensors in the range. The time interval is at least an order of magnitude smaller than the small-scale buoyancy period. This determination is similar to a method used by *Pinkel* [1981] for near-surface data to avoid tracking single isotherms that wander in and out of the observational range and which are ambiguous across unstable overturns. However, *Pinkel* used shorter vertical ranges O(10 m) than employed here. The present method results in a vertically mean time series $\overline{w}(t)$, from which, by integration, a vertically mean isotherm displacement $\overline{\eta}(t)$ can be computed. Naturally, this method does not provide direct w measurements and it also cannot distinguish temperature variations due to local advective and diffusive processes. However, it does give some insight in the large-scale coherent internal wave motions.

[38] The spectrum of this w, dropping the overbar, shows a distinct internal wave band with clear inertial and tidal peaks and a very clear near-N bulge (Figure 9). This near-N bulge in the w spectrum resembles ADCP measurements of w averaged across effective vertical scale of ~20 m, with precisely the same peak frequency and a more rapid roll-off into noise at $\sigma = 4f_h$ as observed above Great Meteor Seamount at 30°N, 28°W [*van Haren*, 2008a]. Our present ADCP data do not resolve N (see below).

[39] The N bulge or band is also observed in the distribution psd(N) of very-small−scale N_s between $\sigma \approx 4f_h$ and N_t, but in the w spectrum its low-frequency increase seems to continue almost smoothly between f and $4f_h$, in a straight slope σ^{+1} along the continuum. The enhanced w level abruptly

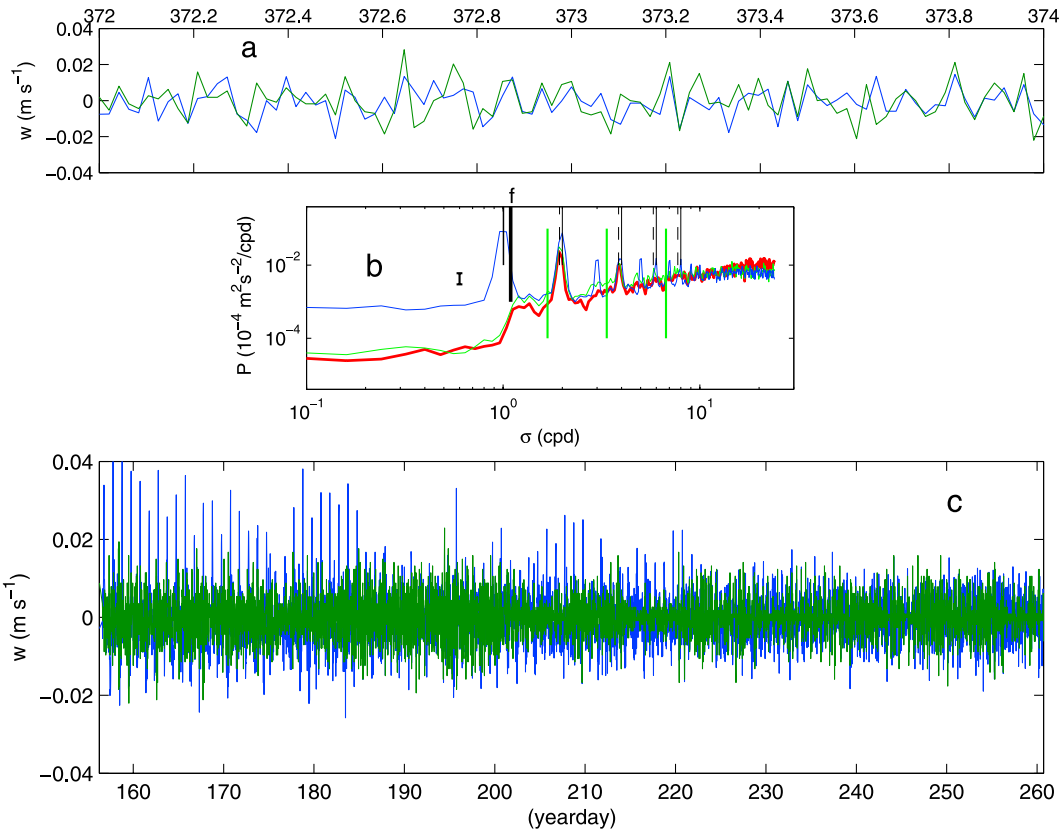

Figure 10. Comparison between w_T computed using temperature data from the 75-kHz acoustic Doppler current profiler (green) just above NIOZ3 and w directly observed using the first 25 bins (250 m vertical average, including NIOZ3-range) of the ADCP (blue, w_{adcp}). The ADCP sampled once per 1800 s. (a) Arbitrary 2-day detail demonstrating reasonable correspondence at high frequencies. (b) Spectra of 1.5 years of data. In red for reference, the w estimate from Figure 9 at 1390 m, subsampled at 1800 s. (c) First 2 months of time series demonstrating diurnal contamination of w_{adcp} data due to plankton motions.

starts at $\sigma = f$, with a peak at the super-inertial side of f. The near-N bulge peaks, for both w and very-small–scale N distribution, at $\sim 0.8N = 0.5N_{\mathrm{m,max}}$ (Δz = 10 m), beyond which frequency it rapidly descends. Fastest roll-off is for $\sigma > N$ around $\sigma = N_t$.

[40] On the other side of the internal wave band, the sudden roll-off for $\sigma < f$ suggests that these subinertial motions are not well monitored by coherent motions. Especially on that side of the spectrum, direct acoustically measured $\mathrm{w_{ADCP}}$ data are ambiguous, due to large noise and due to contamination by vertical plankton migrations that show a strong peak at diurnal and higher harmonic frequencies, also at these great depths in the absolute dark (Figure 10a) and [*van Haren*, 2007].

[41] The above lack of subinertial coherent motions is also found by simply considering a linear heat equation $w_T = -\partial T/\partial t/\langle \mathrm{d}T/\mathrm{d}z \rangle$ [*Krauss*, 1966], where the brackets denote the time mean (Figure 9). Results differ by less than 10% when the mean vertical gradient is replaced by its time-dependent equivalent (Figure 9). Variations due to $\mathrm{d}T/\mathrm{d}z(t)$ do occur, but with persistent layers of alternating relatively thick, weakly stratified and thin, strongly stratified layers the effects are small compared to variations due to $\partial T/\partial t$. It is noted that small Δz = 5 m is used for computing the vertical gradients and all inversions and homogeneous values are ignored in the computation. Apparently, stratification is similar in different step layers, as grouping around N suggests (Figure 9). As a result, a passage from a weakly stratified layer to the next gives almost the same gradient value, with a short passage of higher values in between. This w_T spectrum closely follows w computed from mean displacements for $\sigma \leq 4f_{\mathrm{h}}$, provided a $\langle \partial T/\partial z \rangle \approx 0.9$°C/100 m is taken, which is the highest mean value, that is from the top of the range of Figure 2. Apparently, the coherent motions are governed by the largest buoyancy frequency in the segment, over the range of large-scale N_{l}. For $\sigma > 0.7$ N the discrepancy between the different vertical current estimates becomes rapidly larger, due to the "coherent filtering" inherent to the method of vertical displacement determination that suppresses super-buoyancy motions.

[42] Time series of w_T and directly observed $\mathrm{w_{ADCP}}$ show discrepancies (Figure 10b), partially due to the aforementioned plankton motions, besides locally comparable near-N motions (e.g., Figure 10c). It is noted that the ADCP sampling barely resolves N. Nevertheless, the comparison between w_T using ADCP's temperature sensor and coherent w from NIOZ3 is remarkably good. Periods with large w activity occur in winter. This results in more smooth T spectral roll-off beyond N (months 11 and 12 in Figure 11). However, this may also be related to a passage of a Meddy.

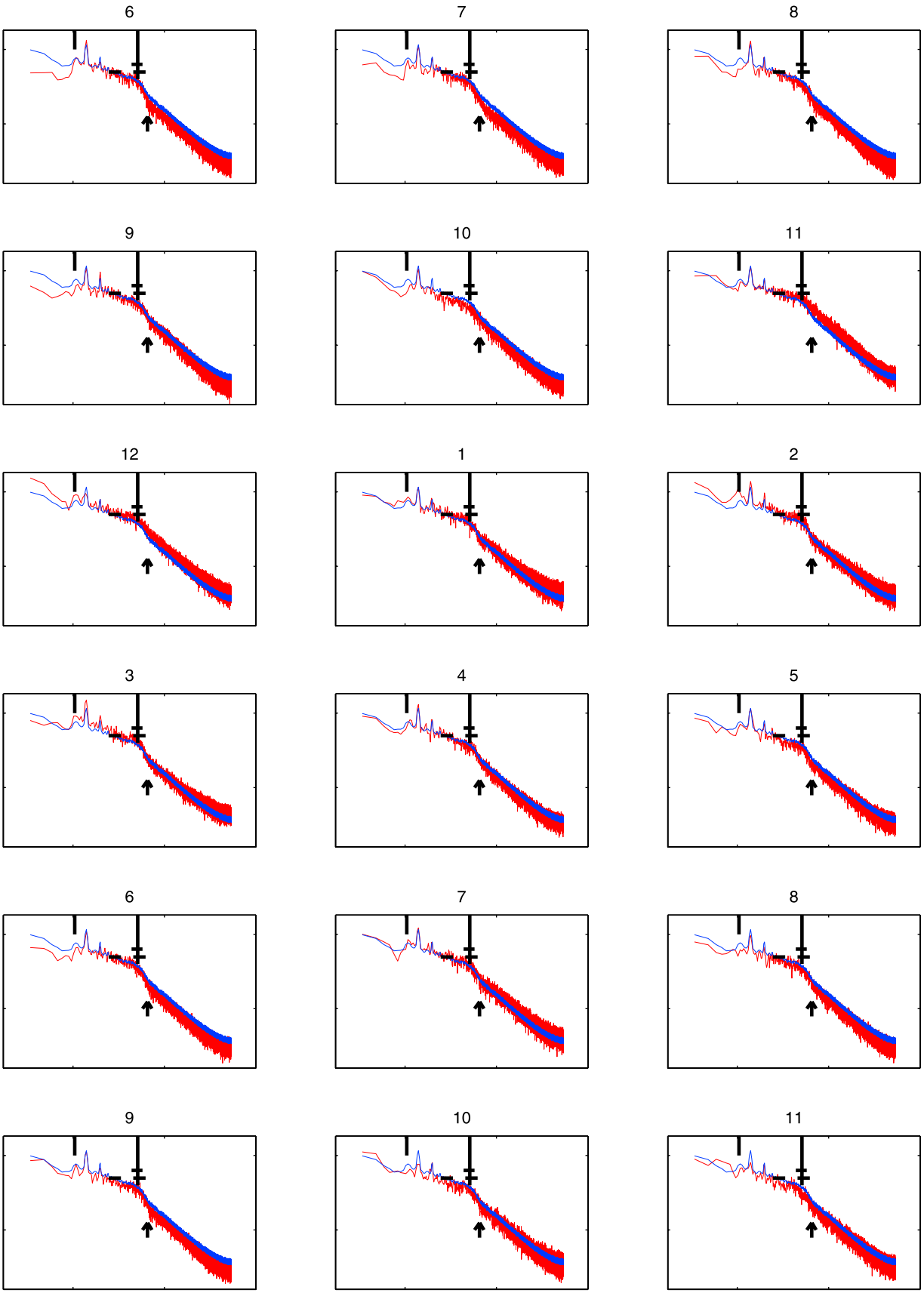

Figure 11. Monthly spectral variation of 15-s subsampled temperature data observed at 1390 m. Months are indicated by numbers, starting with 06 = June 2006. In blue, the 1.5-years long average, for reference. The arrow indicates N_t, the vertical bar f, the "cross bar" N.

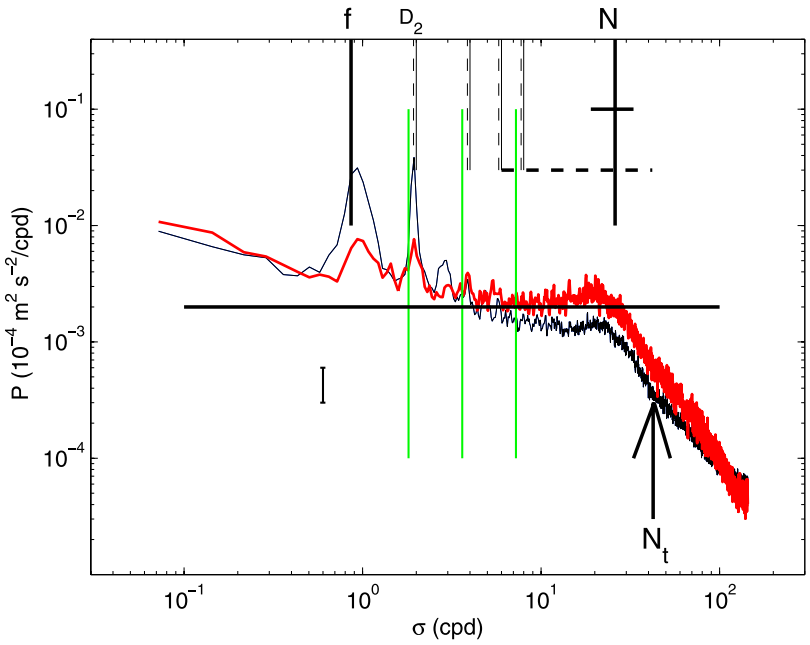

Figure 12. Current (black) and temperature difference (red, arbitrary scale with unit °C^2/cpd) spectra from Valeport mechanical current meter observations. The instruments sampled at once per 300 s for 1.5 years. They were at 1500 and 1502.5 m on position 25.5°N, 24.9°W (H = 5160 m water depth) in the Canary Basin.

Otherwise, monthly variations are not large over the 1.5 years period. No distinct coupling between $T(f)$, $T(D_2)$ and $T(\sigma > N)$ are observed from these plots, except for a tendency of larger $T(f)$ during months 12-03 and of $T(N)$ during 11-03, and, as an exception both larger during summer-month 07, 2007.

5. Discussion

[43] We presented new detailed temperature observations from the deep ocean using very accurate sensors on a nearly stiff mooring. The spectra show a lack of spectral slopes at a −2 fall-off rate. Instead, the internal wave band continuum of T variance falls off at a rate of −1 with frequency. The data also show a prominent internal wave band above a gradually sloping continuum. This extent or elevation commences just at the subinertial side of the inertial frequency and continues to frequencies beyond the large-scale buoyancy frequency, that is to frequencies associated with small-scale local stratification.

[44] It has been suggested by, e.g., *Phillips* [1971] that the transition to [motions at] frequencies outside the above internal wave band are associated with "steps" in vertical temperature profiles, which cause a particular time series $T(t)$ at a certain depth to show abrupt changes in temperature. Principally, finite length series of such steps would yield a −2 sloping spectrum when Fourier transformed. Such has not been observed here, except at very high frequencies, although the time series show very steppy temperature variations. One way to avoid spectral "fine structure contamination" by steps is transforming $T(z, t)$ to a series of isotherm displacements $\eta(z, t)$ and then computing potential energy spectra from them. However, as displacements may wander out of the observational range for long records, a more practical method is by tracking displacements over a certain vertical range from one time step to the next.

[45] This has been done by, e.g., *Pinkel* [1981] for 12 days of near-surface data. His w spectra (in his Figures 2 and 3; and more clearly outlined in Figure 2 of *Gargett and Holloway* [1984]) for O(10 m) vertically smoothing, or one order of magnitude smaller than used here, show resemblance with our w spectra (Figure 9), but also some noteworthy differences. In both, a sudden increase in variance is found by one decade for $\sigma > f$, as well as a smooth continuum above which a near-N bulge extends by a factor of 2 in variance, followed by a sudden decrease by more than one decade for $\sigma > N$. Especially the latter strong decrease indicates that smoothed isotherm following coordinates simply filter coherent from noncoherent w data. This is understood, because all turbulent and inversion closed contours (Figure 3) are just ignored by following a particular contour. What is left is a coherent internal wave band.

[46] Major differences between the near-surface data and our deep-ocean data by *Pinkel* [1981] are as follows. Firstly, a σ^{+1} sloping continuum in our w data for $f < \sigma < 0.8$N, compared to σ^0 in *Pinkel*'s data, and, hence, a larger near-N bulge in NIOZ3 data. This results in a σ^{-1} slope when transformed into a displacement spectrum rather than σ^{-2} slope as found by *Pinkel* and by *Cairns and Williams* [1976]. Secondly, the near-inertial peak extends to lower frequencies in our data: the spectrum of *Pinkel* [1981] falls off for $\sigma < D_2$, which is significantly away from $\sigma = f$. This may be because *Pinkel* was measuring from a drifting platform, like *Cairns and Williams*, thereby annihilating some of the inertial motions. Perhaps this also affected the continuum slope. Or, near the surface inertial (slantwise) convection is not very important at subtropical latitudes. This requires some further investigation.

[47] Similarly, the importance of small-vertical−scale stratification should be further investigated, for example in comparison with small-scale shear. A particular coupling

does seem to exist between the shapes of ΔT and shear, actually vertical current difference, spectra across $\Delta z = 2.5$ m (Figure 12). These data were also obtained over the same 1.5 years as NIOZ3, but at 1500 m at a more southerly mooring ($\sim$25°N) in the Canary Basin. There, shear is observed non-negligible at the tidal frequency and also, largest, inertial shear is extending above continuum noise level. It is noted that these data from mechanical current meters are not perfect, especially for motions at inertial/tidal frequencies, due to frictional impellors. Near the buoyancy frequency however, data are much better than can be obtained with most acoustic devices. In the N band it is seen that the shear spectrum complies well with the buoyancy estimates: the shear shows a local internal wave band minimum near $\sigma = 4f_h$, beyond which the spectrum weakly increases with increasing frequency to a submaximum at $\sim$0.8N $\approx$ 20 cpd, basically coinciding in frequency with the ΔT peak (Figure 12) and the w peak (Figure 9). The roll-off for $\sigma = N_t$, indeed the same transition as found for T and ΔT, is well indicated, so that the shear spectrum also seems affected by small-scale stratification, which it may help maintaining.

[48] We conclude that the deep ocean of the Canary Basin is not a smoothly stratified medium, but a layered, steppy field of density variations that is permanently in motion. This can be observed in vertical CTD profiles, but is also apparent in long-term accurate thermistor string time series, as presented. The density layering is also reflected in spectra, inferred from such time series. It determines the subinertial internal wave extent of the spectrum, the continuum internal wave band slope, notably in vertical currents, and the bulge near the buoyancy frequency. Once set in motion, particular layered large- and small-scale density gradients determine coherent and incoherent quasi-interfacial wave motions. One of the remaining key problems is how this motion is started.

[49] **Acknowledgments.** We thank the crew of the R.V. Pelagia for deployment and recovery of the mooring. We enjoyed discussions with Martin Laan on all aspects of NIOZ' thermistor strings. We thank Bill Merrifield for advice and referees for their criticism. The construction and deployment of NIOZ3 were financed by investment grants ("Oceanographic equipment" and "LOCO", respectively) from the Netherlands organization for the advancement of scientific research, NWO.

References

Antonov, J. I., R. A. Locarnini, T. P. Boyer, A. V. Mishonov, and H. E. Garcia (2006), *World Ocean Atlas 2005, Volume 2: Salinity*, edited by S. Levitus, 182 pp., NOAA Atlas NESDIS 62, US Govt. Print. Off., Washington, D. C.

Briscoe, M. G. (1975), Preliminary results from the trimoored Internal Wave Experiment (IWEX), *J. Geophys. Res.*, *80*, 3872–3884.

Cairns, J. L., and G. O. Williams (1976), Internal wave observations from a midwater float. 2, *J. Geophys. Res.*, *81*, 1943–1950.

Davis, R. E., and A. Acrivos (1967), Solitary internal waves in deep water, *J. Fluid Mech.*, *29*, 593–607.

Elliott, A. J., M. R. Howe, and R. I. Tait (1974), The lateral coherence of a system of thermo-haline layers in the deep ocean, *Deep Sea Res.*, *21*, 95–107.

Gargett, A. E., and G. Holloway (1984), Dissipation and diffusion by internal wave breaking, *J. Mar. Res.*, *42*, 15–27.

Garrett, C. J. R., and W. H. Munk (1972), Space-time scales of internal waves, *Geophys. Fluid Dyn.*, *3*, 225–264.

Garrett, C., and W. Munk (1979), Internal waves in the ocean, *Ann. Rev. Fluid Mech.*, *11*, 339–369.

Gerkema, T., and V. I. Shrira (2005), Near-inertial waves in the ocean: Beyond the "traditional approximation", *J. Fluid Mech.*, *529*, 195–219.

Gregg, M. C. (1977), Variations in the intensity of small-scale mixing in the main thermocline, *J. Phys. Oceanogr.*, *7*, 436–454.

Holloway, G. (1986), Considerations on the theory of temperature spectra in stably stratified turbulence, *J. Phys. Oceanogr.*, *16*, 2179–2183.

Howe, M. R., and R. I. Tait (1970), Further observations of thermo-haline stratification in the deep ocean, *Deep Sea Res.*, *17*, 963–972.

Krauss, W. (1966), *Methoden und Ergebnisse der Theoretischen Ozeanographie. II: Interne Wellen*, 248 pp., Gebrueder Borntraeger, Berlin, Germany.

LeBlond, P. H., and L. A. Mysak (1978), *Waves in the Ocean*, 602 pp., Elsevier, New York.

Oakey, N. S. (1982), Determination of the rate of dissipation of turbulent energy from simultaneous temperature and velocity shear microstructure measurements, *J. Phys. Oceanogr.*, *12*, 256–271.

Osborn, T. R. (1980), Estimates of the local rate of vertical diffusion from dissipation measurements, *J. Phys. Oceanogr.*, *10*, 83–89.

Phillips, O. M. (1971), On spectra measured in an undulating layered medium, *J. Phys. Oceanogr.*, *1*, 1–6.

Pinkel, R. (1981), Observations of the near-surface internal wavefield, *J. Phys. Oceanogr.*, *11*, 1248–1257.

Schuster, H. G. (1984), *Deterministic Chaos, an Introduction*, 220 pp., Physik-Verlag, Weinheim, Germany.

Siedler, G. (1974), Observations of internal wave coherence in the deep ocean, *Deep Sea Res.*, *21*, 597–610.

Sreenivasan, K. R. (1996), The passive scalar spectrum and the Obukhov-Corrsin constant, *Phys. Fluids*, *8*, 189–196.

Straneo, F., M. Kawase, and S. C. Riser (2002), Idealized models of slantwise convection in a baroclinic flow, *J. Phys. Oceanogr.*, *32*, 558–572.

Tennekes, H., and J. L. Lumley (1972), *A First Course in Turbulence*, 300 pp., MIT Press, Cambridge, Mass.

van Haren, H. (2004), Bandwidth similarity at inertial and tidal frequencies in kinetic energy spectra from the Bay of Biscay, *Deep Sea Res. I*, *51*, 637–652.

van Haren, H. (2007), Monthly periodicity in acoustic reflections and vertical motions in the deep ocean, *Geophys. Res. Lett.*, *34*, L12603, doi:10.1029/2007GL029947.

van Haren, H. (2008a), Self-regulation of deep-ocean internal wave continuum: Observations on related near-inertial shear and high-frequency vertical motions, *Geophys. Res. Lett.*, *35*, L04606, doi:10.1029/2007GL032697.

van Haren, H. (2008b), Abrupt transitions between gyroscopic and internal gravity waves: The mid-latitude case, *J. Fluid Mech.*, *598*, 67–80.

Webster, F. (1972), Estimates of the coherence of ocean currents over vertical distances, *Deep Sea Res.*, *19*, 35–44.

Weinstock, J. (1985), On the theory of temperature spectra in a stably stratified fluid, *J. Phys. Oceanogr.*, *15*, 475–477.

Wunsch, C., and S. Webb (1979), The climatology of deep ocean internal waves, *J. Phys. Oceanogr.*, *9*, 235–243.

Zenk, W. (1970), On the temperature and salinity structure of the Mediterranean water in the Northeast Atlantic, *Deep Sea Res.*, *17*, 627–631.

L. Gostiaux, Coriolis-Laboratoire des Ecoulements Geophysique et Industriels, CNRS, 21 rue des Martyrs, F-38 000 Grenoble, France.

H. van Haren, Royal Netherlands Institute for Sea Research (NIOZ), Physical Oceanography, P.O. Box 59, NL-1790 AB Den Burg, Netherlands. (hansvh@nioz.nl)